JOINT EUROPEAN TORUS

JET–P(91)03

J.P. Christiansen, J.G. Cordey, O. Kardaun, K. Thomsen
and JET Team

# Application of Plasma Physics Constraints to Confinement Data

# Application of Plasma Physics Constraints to Confinement Data

J.P. Christiansen, J.G. Cordey, O. Kardaun[1], K. Thomsen
and JET Team*

***JET-Joint Undertaking, Culham Science Centre, OX14 3DB, Abingdon, UK***

*[1]IPP Garching, Germany*
** See Appendix 1*

Preprint of Paper to be submitted for publication in
Nuclear Fusion

# Application of plasma physics constraints to confinement data

J.P. Christiansen, J.G. Cordey, O. Kardaun*, K. Thomsen
JET Joint Undertaking, Abingdon, Oxfordshire, OX14 3EA, England.

*IPP Garching, Germany.

Abstract

A subset of the ITER L and H-mode confinement data is tested against the constraints imposed by various theoretical models for thermal plasma transport. Matrix algebra is used to facilitate such tests. A new result obtained is that the fundamental constraint imposed by the High-β collisional Fokker Planck equation (Kadomtsev) is satisfied by the data. An additional constraint on the characteristic scale length associated with thermal diffusion can also be satisfied by the data. Dimensionally correct empirical scaling laws embodying theoretical constraints can thus be derived.

## 1. Introduction

Studies of data from one or more Tokamak experiments have produced a large number of empirical scaling laws for the energy confinement time $\tau_E$. When such scaling laws are used in extrapolations to proposed experiments like ITER [1] or CIT [2] a wide range of estimates for $\tau_E$ will arise in the sense that some scaling laws predict ignition while others do not. A high level of confidence in an extrapolation requires a considerable variation in the values of the data used. The largest such variations can be found in the ITER L-mode data base [3] and the ITER H-mode data base [4]; these two data bases represent the most comprehensive Tokamak data assembled so far. However, extrapolations to the proposed ITER experiment [1] based upon these data bases embody significant uncertainties. The L-mode data extrapolations are discussed in [5,6] while an analysis of the H-mode data has been presented recently [7].
Empirical scaling laws like the Goldston scaling [8] or the Kaye-Goldston scaling laws [9] as well as those of [1-6] are usually cast as a power law expression involving "engineering" variables

$$\tau_E = C\, a^{z_a}\, n^{z_n}\, I^{z_I}\, P^{z_P}\, \varepsilon^{z_\varepsilon}\, \kappa^{z_\kappa}\, B^{z_B}\, A^{z_A} \cdots \qquad (1)$$

The constant C and the exponents $z_k$ are determined from statistical fits of data on $\tau_E$ to the data on minor radius a, density n, current I, power P, inverse aspect ratio ε,

elongation $\kappa$, field B, ion mass A etc. There is no theoretical justification for the power law form (1) and many authors have instead employed an off-set linear form [10,11].

A recent study [12] has shown that most empirical scaling laws expressed in the form (1), each law having particular values for the exponents $z_k$, possess a set of common physics features. Such features are derived from the Connor-Taylor scale invariance approach to confinement scaling [13] and they are expressed by

$$\tau_E = C\ \tau_B\ f(\rho_*, \nu_*, \beta, \varepsilon, \kappa, q, A, \lambda_D, \lambda_T, \lambda_n,) \qquad (2)$$

In this dimensionally correct scaling expression for the confinement time C is a constant, $\tau_B$ is the Bohm time and f is some function of the dimensionless physics variables which will be defined later; $\rho_*$ and $\nu_*$ denote normalised Larmor radius and collsionality; $\beta$ is plasma beta; $\lambda_D$, $\lambda_T$, $\lambda_n$, $\lambda_s$ denote Debye length, profile length scales of T, n and B all normalised to minor radius a. Several of the variables in (2) depend on $\tau_E$ such that Eq. (2) is an implicit equation for $\tau_E$. A previous study [12] has demonstrated that with minor changes $\delta z_k$ to $z_k$, many of the empirical scaling laws of type (1) can be cast in the form (2) with specific dependencies upon $\rho_*$, $\nu_*$ and $\beta$. Plasma physics theories for thermal transport predict specific dependencies of $\tau_E$ upon the arguments of the function f in (2) as explained in the review by Connor [14]. The work presented in this paper addresses the question whether the constraints imposed by theories are satisfied by the data presently available.

The main result obtained from a comprehensive series of analyses of L and H-mode data from a variety of Tokamak experiments is that global confinement data satisfies the fundamental constraint imposed by the High-$\beta$ collisional Fokker Planck equation. This constraint, which was first derived by Kadomtsev [15] requires that $\tau_E$ can be expressed as (2) but without any dependence upon the Debye length $\lambda_D$ [6]. Thus plasma physics effects characterized by scale lengths of order the Debye length are not important for thermal transport. The scaling of the energy confinement time in a Tokamak thus has a firm physic foundation. It also puts on a firm basis the "wind tunnel like" experiments proposed by Waltz [16]. Additional theoretical constraints on the dependence of $\tau_E$ upon $\rho_*$, $\nu_*$, $\beta$ etc. are also tested against the data. The scaling expression used to implement such tests is a power law expression

$$\tau_E = C\ \tau_B{}^{x_\tau} \rho_*{}^{x_\rho}\ \nu_*{}^{x_\nu}\ \beta^{x_\beta}\ \varepsilon^{x_\varepsilon}\ \kappa^{x_\kappa}\ q^{x_q}\ A^{x_A} \ldots \qquad (3)$$

Imposing theoretical constraints on the form (3) corresponds to assigning definite values for the exponents $x_k$: the Kadomtsev constraint [15] requires $x_\tau = 1$ as an example. The methods of analysis and six theoretical models for thermal plasma

transport are presented in four Appendices and many numerical results are given in five Tables while the paper itself describes the main results of our analysis.

In section 2 we present a summary of the ITER L and H-mode data. For clarity we emphasize the data selection criteria we have employed; these criteria largely correspond to those of [6,7,12]. The difference between the scaling of *thermal* ($\tau_E = \tau_{thermal}$) and *total* ($\tau_{total}$) energy confinement time is emphasized. The Appendices present some features of multivariate analysis techniques [17] required for our analysis.
Section 3 and Appendix 1 defines the variables of Eqs. (1) and (2) used in the analysis. If a power law expression such as (1) is assumed to depict variations in confinement time then all the algebra relating one set of variables to another becomes linear. Appendix 2 presents features of the regression techniques.
Section 4 describes some shortcomings of the L and H-mode data. A principal component analysis is made to investigate collinearities in the data on both dimensional and dimensionless variables.
The statistical method employed to test whether a theoretical constraint is satisfied, is the F-test [17] and the problems associated with this test are discussed in section 5 and Appendix 3.
In section 6 and Appendix 4 we consider six theoretical models for thermal transport in a plasma; the models are described in more detail by Connor [14]. The constraints imposed by each model are examined and tested against the ITER L and H-mode data.

The results obtained in section 6 lead to the conclusion: i) global confinement data can always be represented in dimensionally correct physics forms [13, 15]; ii) careful estimates of the global thermal energy content enable us to determine the length scale, associated with thermal diffusion; iii) the dependencies of confinement time upon additional parameters describing collisionality $\nu_*$, $\beta$, safety factor q etc. cannot accurately be determined from global data in its present form; a more refined analysis based on local data [18] is required.

## 2. Summary of data bases

The ITER L-mode data base contains 1431 sets of data (observations) from JET, TFTR, JT-60, DIII-D and JFT2 and it has been assembled by S.M. Kaye [3]. This data base has already been used for confinement analysis [5,6]. The ITER H-mode data base [4] contains 3482 data sets of data from JET, DIII-D ASDEX, PDX, PBX and JFT2 and has been assembled recently. This data base includes per dataset a more extensive list of variables than the L-mode database. The variable set used for the study presented in this paper is therefore the common subset of the two databases; it means that variables like electron temperature, wall-limiter material, plasma shape (except elongation) etc. will be excluded. Table I summarizes the data on a number of relevant plasma parameters by giving their range, i.e. the minimum and maximum values found in the data bases, and the associated symbols used in this paper. Also included in Table I is a number of dimensionless parameters which will be defined in the next section.

The data to be used is selected from both databases as follows. Only data with neutral beam heating (NBI) as auxiliary heating is considered; H-mode data with ELM's is not used. Furthermore we impose the following conditions adopted in [4, 6, 7, 12]

$$\frac{W_f}{W} < 0.4 \quad , \quad -0.05 < \frac{1}{P}\frac{dW}{dt} < 0.35 \quad , \quad \frac{P_{rad}}{P} < 0.6 \quad , \quad q_{95} > 3.1 \qquad (4)$$

The fast ion energy $W_f$ will be defined below. The total plasma energy W is based on MHD fits but for JET and ASDEX we use $W = W_{dia}$, the latter being based on diamagnetic measurements available only for H-mode data. The net input power P is defined as

$$P = P_{OH} + P_{abs} - \frac{dW}{dt} = \frac{W}{\tau_{total}}$$

where $P_{abs}$ denotes the absorbed beam power. There is no data in the L-mode data base for the time derivative of W nor is there data for the radiated power $P_{rad}$. The following number of datasets for each machine, which results from the conditions (4) becomes (the total number is denoted by N):

For the L-mode data base N = 680 distributed as JET (353), TRTR (67), JT-60 (209), DIII-D (5), JFT2 (46).

For the H-mode data base N = 693 distributed as JET (246), DIII-D (34), ASDEX (16), PDX (24), JFT2M (218), PBXM (155).

The restrictions (4) omit TFTR supershots (L-mode) and extreme non-steady H-mode data.

In order to prepare data on thermal confinement from the selected subsets of data we need to estimate the fast ion energy content. This energy content is obtained using the approximate expression

$$W_f = P_{abs}\ \tau_s / 2 \quad , \quad \tau_s = \frac{1}{3}\ 3.7\ 10^{13}\ \frac{T^{3/2} A_b}{n}\ \log\left(1+\left(\frac{E_b}{E_c}\right)^{3/2}\right) \qquad (5)$$

The expression for the slowing down time $\tau_s$ can be found in the literature, e.g. [19]. The critical energy is given by

$$E_c = 14.8\ T\ \frac{A_b}{A^{2/3}}$$

For the L-mode data the average temperature T is defined as

$$T = \frac{W}{2.1 e n V} \quad , \quad V = 2\pi^2 a^3 \kappa \varepsilon^{-1} \qquad (6)$$

The factor 2.1 arises from a fit to both JET and ITER H-mode data for T. Values of $W_f$ given by Eq. (5) agree very well with the estimates made for the ITER H-mode data base even though Eq. (5) is only approximate, i.e. no profile effects etc. are included. The total and the thermal energy confinement times are defined by

$$\tau_{total} = \frac{W}{P} \quad , \quad \tau_{thermal} = \tau_E = \frac{W - W_f}{P} = \tau \qquad (7)$$

For L-mode data we use Eq. (5) for $W_f$ ; for H-mode data we employ the estimates for $W_f$ given in the database. For brevity we use $\tau$ instead of $\tau_E$ in the following.

## 3. Variables

The variables used in our study are those 8 independent variables of Eq. (1). The variable set denoted by a vector $\underline{Z}$ in the Appendix is referred to as the engineering set. The data range for these variables is given in Table I. From the set $\underline{Z}$ we can derive [9, 16] the following variables used in Eq. (2)

$$\tau_B \sim \frac{a^4 n I \kappa}{\varepsilon P \tau} \quad , \quad \rho_* = \rho / a \sim \left( \frac{\varepsilon P \tau A}{a^3 n I^2 \kappa} \right)^{1/2} \tag{8}$$

$$\nu_* \sim \frac{a^7 n^3 \kappa^2}{\varepsilon^3 P^2 \tau^2} \quad , \quad \beta \sim \frac{\varepsilon P \tau}{a I^2} \tag{9}$$

$$\varepsilon = \frac{a}{R} \quad , \quad \kappa = \frac{b}{a} \quad , \quad q \sim \frac{\varepsilon a \kappa B}{I} \tag{10}$$

The ranges for these variables are also given in Table 1 together with their associated variances $s_k$ defined in Appendix 1. The choice of a timescale (8) $\tau_B \sim a/I\ \rho_*^{-2}$ is equivalent to the conventional choice which replaces $\tau_B$ by $B^{-1}$ or a/I [6,16]. The set of variables (8 - 10) is denoted by a vector $\underline{X}$ and it is referred to as the physics set.

Many more variables may be relevant to confinement studies, e.g. $Z_{eff}$ or $\lambda_n$, $\lambda_T$, $\lambda_s$ of Eq. (2). In addition the neutral beam heating efficiency $\eta$ [20] could be included to account for the degree of beam penetration in the various Tokamaks; $\eta$ depends on the density profile and an assumed heat diffusivity profile. Such variables are however not available in the databases.

## 4. Collinearities in the data

Considerable simplifications occur if the regression analysis (see Appendix 2) is made on a set of orthogonal variables. It means that the variables of (1) should have been varied completely independently of each other. For practical and experimental reasons this is however not the case. Both ITER L and H-mode data exhibit inner relations or collinearities. For instance

i) Density n is proportional to current I for one Tokamak
ii) Power P and current I are correlated with machine size R
iii) Field B and current I are also related to R

As an example of data collinearity we show in Figure 1 the L-mode data on $\tilde{\beta}$ plotted against that of $\tilde{\rho}_*$; Figure 2 shows H-mode data on $\tilde{\beta}$ versus that of $\tilde{\nu}_*$; both Figures are log-log plots. The tilde symbol, e.g. $\tilde{\beta}$, means that $\tau$ is omitted from the definitions (8-9) such that the variables plotted in Figs. 1 and 2 are the actual regressor variables (see Appendix 1). It is clear from these Figures that the variables are not orthogonal and that a "trade-off" between the associated exponents $x_k$ of Eq. (2) is possible in regression fits. To asses the influence of collinearity on estimates of the exponents $x_k$ (or $z_k$) we carry out a principal components analysis on the L and H-mode data separately; the

details are given in Appendix 1. The analysis yields a set of orthogonal components and Tables II and III summarize their content. The relations of Appendix 1 can be employed to express the orthogonal components in terms of the four sets of variables considered. Tables II and III also include the results for the regression fits described in Appendix 2.

## 5. Does the data satisfy a theoretical constraint

A theoretical constraint on the scaling of the thermal confinement time requires that the expression (2) can be cast as the product of a leading term $\tau_{theory}$ in place of $\tau_B$ and some function f of dimensionless plasma parameters. The leading term $\tau_{theory}$ embodies K constraints which arise from the scale invariance of the plasma physics equations used. The most fundamental constraint is that of the collisional High-$\beta$ model of Kadomtsev [15] based on a Fokker-Planck equation which yields the scaling expression (2). This constraint eliminates effects on thermal plasma transport arising from radiation, atomic physics and high frequency ($\omega \sim \omega_p$), short wavelength ($\lambda \sim \lambda_D$) oscillations; $\omega_p$ is the plasma frequency.

As mentioned in the introduction Eq. (2) is an implicit equation in $\tau$ and regression fits are therefore made to the explicit form derived from (3)

$$\tau = C \;\; \tilde{\tau}_B^{\,y_\tau} \;\; \tilde{\rho}_*^{\,y_\rho} \;\; \tilde{\nu}_*^{\,y_\nu} \;\; \tilde{\beta}^{y_\beta} \;\; \varepsilon^{y_\varepsilon} \;\; \kappa^{y_\kappa} \;\; q^{y_q} \;\; A^{y_A} \qquad (11)$$

where the tilde symbol denotes the omission of $\tau$ from Eqs. (8-9). Eqs. (3) and (11) are equivalent and the fundamental constraint of Kadomtsev [15] can be expressed as

$$x_\tau = 1 \qquad or \qquad 2y_\tau - \tfrac{1}{2}\, y_\rho + 2y_\nu - y_\beta = 1 \qquad (12)$$

All theoretical models include this fundamental constraint but impose additional constraints on the exponents $x_\rho$, $x_\nu$, $x_\beta$ etc. Appendix 2 shows that the x and y exponents are linearly related. Hence all theoretical constraints can be expressed via linear equations such as (12) and imposed on the regression equation (11). Appendix 4 presents several constraints equations. Formally these are expressed by

$$\underline{C}\;\underline{x} = 0 \qquad (13)$$

where for the general case of K constraints $\underline{C}$ is a K by M + 1 constraint matrix acting on the vector of M + 1 exponents $\underline{x}$. The example (12) thus corresponds to $\underline{C}$ = (110000000). Two constraints can be imposed by the short wavelength gyrokinetic scaling which requires a dependence as $\rho_*^{-1}$ in (11); in this case $\underline{C}$ becomes (see Appendix 4)

$$\underline{C} = \begin{pmatrix} 110000000 \\ 011000000 \end{pmatrix}$$

and so forth. From the relations of Appendix 2 Eq. (12) can also be expressed in terms of the exponents for other variable representations. The fundamental constraint (12) is equivalent to the representation

$$4\,z_a - 8\,z_n - z_I - 3\,z_p - 5\,z_B = 5 \qquad (14)$$

The coefficients 4, -8, -1 etc in (14) are the constraint coefficients arising from the definitions (8-9). To assess if (14) can be satisfied by experimental data the dimensional parameters a, n, I, P and B must show significant variations; this is the case for the ITER L and H-mode databases.

If K constraints are imposed on regression fits involving M independent variables then the number of degrees of freedom in the fits is reduced from M to M-K. From a statistical point of view such a reduction is acceptable if

$$(\underline{C}\,\underline{x})^t \left[\underline{C}^1 \underline{S} \underline{C}^1\right]^{-1} \underline{C}\,\underline{x} \;<\; F(\mathrm{K}, N-M+\mathrm{K}, \alpha) \qquad (15)$$

The inequality represents the F-test [17] for a confidence level $\alpha$ in a fit to M-K independent variables with N data values. $\underline{S}$ is the data covariance matrix associated with $\underline{x}$; to apply the test (15) we need to substitute $\underline{x}$ by $\underline{y}$ or $\underline{z}$ via the relations of Appendix 2 and substitute $\underline{S}$ by the appropriate covariance matrix. Equivalent, but simpler forms of the test (15) can be derived for large N [17], say N > 100. The F-test can in this case be expressed as

$$\Delta\sigma^2 \;=\; \sigma_C^2 - \sigma_U^2 \;<\; \frac{e_\tau^{\,2}}{N_s} \;=\; \Delta\sigma^2_{\max} \qquad (16)$$

where subscripts C and U refer to mean square errors for constrained and unconstrained regression fits respectively. The mean square error is defined as

$$\sigma^2 = \frac{1}{N-M+K} \sum_{j=1}^{N} \left(\log \tau - \log \tau_{\mathrm{fit}}\right)_j^2$$

where $\tau_{\mathrm{fit}}$ denotes the value obtained from e.g. (11).

The F-test assumes that the error $e_\tau$ on $\tau$ is of order $\sigma_U$ and that the number $N_s$ of *independent* measurements is N.

The test (15) or (16) is rather strict as emphasized in [5]. We believe (but cannot prove) that $e_\tau > \sigma_U$ and that $N_s << N$. Reference [5] suggests $N_T < N_s < N$, where $N_T$ denotes the number of different Tokamaks. The problem of choosing appropriate values for $e_\tau$ and $N_s$ remains presently unresolved and we proceed with the conservative *estimates* that the errors on $\tau$ are not systematic but random and characterized by $\sigma_U$; we also assume that the number of independent measurements $N_s$ is the number of data values N. The implication for the ITER L and H-mode data for which $\sigma_U = 0.096$ and 0.124 respectively is that $(\Delta\sigma^2_{max})^{1/2} = 8.0\ 10^{-3}$ and $9.0\ 10^{-3}$ respectively; therefore (15) is indeed a strict condition.

## 6. Results for transport models

In Appendix 4 we present the constraint equations of the type (12) and (14) for 6 theoretical models of thermal transport. In this section we just discuss the results from a wide range of computational exercises some of which are listed in Table IV. In the range of exercises we have both included and omitted subsets of data characterized by individual Tokamaks and H-mode data characterized by the presence of ELM's or Giant ELM's etc. The first constraint, that of the High-$\beta$ collisional Fokker Planck model of Kadomtsev presented in the previous section, is common to the $\tau$ scaling expressions derived from the six theoretical models considered. The second constraint concerns the scale length which characterises the turbulent diffusivity $\chi$ and it is imposed by fixing the $\rho_*$ dependence $x_\rho$ in (3). A third constraint describes the dependence of $\chi$ upon collisionality $\nu_*$ and it is imposed via $x_\nu$ of (3). Further constraints, not considered here, could impose an $\eta_i$ [21,22] dependence etc.
Let us first consider the difference between the *total* and the *thermal* energy confinement times both defined by Eq. (7). From the algebra of Appendix 1 it can be shown that

$$\tau_{fast} = C_f\ \tau_B\, \rho_*^{1} \nu_*^{-1} \varepsilon^{-5} \qquad (17)$$

where $C_f$ is some constant. We insert (3) and (17) into (7) and impose the fundamental constraint $x_\tau = 1$ on $\tau = \tau_{thermal}$. This gives

$$\tau_{total} = \tau_B \left[ f(\rho_*, \nu_*, \ldots) + C_f\, \rho_*^{1}\, \nu_*^{-1} \varepsilon^{-5} \right] \qquad (18)$$

The results shown in Table IV confirm that the fundamental constraint is very well satisfied by both the L and the H-mode data for $\tau_{thermal}$. Table IV also confirms that the same applies to the data on $\tau_{total}$ just as Eq. (18) predicts.
We see however from Eq. (18) that to satisfy the additional constraints concerning the scale length $\rho_*$ and collisionality $\nu_*$, we require an accurate estimate of $C_f$, i.e. the fast

ion energy. $C_f$, though formally treated as a constant, will depend on spatial plasma profiles via the neutral beam heating efficiency parameter $\eta$ [20] and such a dependency has been excluded. The second constraint on the $\rho_*$ dependence can be written as (see Appendix 4)

$$-2\, z_a + 14\, z_n + 8\, z_I + 9\, z_p + 10\, z_B = G \qquad (19)$$

where for the short wavelength, long wavelength and resistive MHD scalings G becomes 5, - 5 $z_p$ and - $^5/_2$ (1 + 3 $z_p$ + 2 $z_n$) respectively; typical ranges for G are respectively 5, 3-4 and 1-2. Eq. (19) shows us that changes $\delta z_k$ to the exponents $z_k$ of order only 0.03 - 0.06 are sufficient to change the $\rho_*$ scaling exponent $x_\rho$ from - 1 to 0 or from 0 to 1. Such changes $\delta z_k$ can arise from i) lack of accuracy of $C_f$, ii) different data selections, iii) omission of the least varied principal components. The sensitivity of the constraint on $\rho_*$ can also be seen from Eq. (A2.4) of Appendix 2. The typical values for $x_0$ are $^{-1}/_5$ (L-mode) or $^{-1}/_4$ (H-mode); the errors $\delta x_k$ on $x_k$ are thus 4 to 5 times those of $\delta z_k$. In addition the data collinearities shown in Figs. 1 and 2 permit a "trade-off" in the fits between $x_\rho$, $x_\nu$ and $x_\beta$.
The sensitivity problem just described is brought out by the results in Tables IV and V. For the L-mode data the additional long wavelength gyrokinetic constraint can be marginally satisfied by the $\tau_{thermal}$ data but only if the least principal component no. 8 is retained. On the other hand the resistive and ideal MHD constraints, both predicting a $\rho_*^1$ scaling, are satisfied by the data on $\tau_{total}$. For the H-mode data the additional short wavelength scaling constraint is marginally satisfied by both $\tau_{thermal}$ and by $\tau_{total}$. Hence the variation of $C_f$ with the beam heating efficiency $\eta$ is more pronounced for L than for H-mode data.

In summary the ITER L and H-mode confinement data, as well as subsets thereof, is well described by scaling expressions which embody the fundamental High-$\beta$ Fokker-Planck constraint of Kadomtsev. The scaling expressions also embody constraints on the turbulent diffusivity form whose characteristic scale length is somewhere between the ion Larmor radius (short wavelength gyro-kinetic scaling) and minor radius (long wavelength Bohm scaling). Further scalings of $\tau$ with $\nu_*$, $\beta$ etc. remain speculative in view of the strictness of the F-test employed in this work.

Dimensionally correct scaling expressions for the L and H-mode data can be obtained from the values in Table V. Applying the constraints of various theories will yield a set of scaling laws which, if expressed in the form (1), appear different [12]. Yet their common root is the form (2) embodying the High-$\beta$ Fokker Planck constraint. With this constraint the L and H-mode scaling are very similar and differ only in the $\epsilon$ and B dependencies due to the shortcomings of the data as described in this paper:

$$\tau(L-\text{mode}) = 0.095\ a^{2.02}\ n^{0.41}\ I^{0.79}\ \mathrm{P}^{-0.79}\ \varepsilon^{-0.56}\ \kappa^{0.73}\ A^{-0.02}\ B^{0.29} \qquad (20a)$$

$$\tau(H-\text{mode}) = 0.027\ a^{2.35}\ n^{0.38}\ I^{0.82}\ \mathrm{P}^{-0.75}\ \varepsilon^{-2.05}\ \kappa^{0.58}\ A^{0.29}\ B^{0.55} \qquad (20b)$$

In the two expressions (20a) and (20b) the units are:

$$\tau(s),\ \ a(m),\ \ n\ \left(10^{19}m^{-3}\right),\ \ P(MW)\ \ and\ \ B\ (Tesla).$$

The ranges of uncertainty arising from extrapolations to ITER parameters can be established by applying the scaling expressions (20) together with those that satisfy other constraints (see Table IV). The result is

$$1.01s < \tau_{ITER}\,(L-\text{mode}) < 1.48s \quad , \quad 4.23s < \tau_{ITER}\,(H-\text{mode}) < 4.95s \ .$$

There is little experimental evidence for the strong B scaling in (20b); this is a consequence of the collinearity in the H-mode data as already explained. If the B scaling is fixed, e.g. $B^{0.15}$ or $B^{0.3}$, as made in [7], a scaling expression slightly different from (20b) arises. However, the Kadomtsev and short wavelength constraints are in this case still satisfied.

## 7. Conclusions

The ITER L and H-mode data bases incorporate the most extensive range of Tokamak confinement data assembled so far. A subset of the data, characterized by steady state L and H-mode confinement not too strongly influenced by radiation and sawteeth, has been selected. We have demonstrated that this data always satisfies the fundamental High-$\beta$ Fokker Planck constraint arising from the Connor-Taylor scale invariance approach. In addition we have shown that the thermal confinement time follows a scaling associated with a diffusivity characterized by a scale length somewhere between the ion Larmor radius and the minor radius. The H-mode data is closer to the former while the L-mode data is closer to the latter. We have explained how the uncertainty in pinning down this characteristic scale length results from shortcomings in the data and the inaccuracies in the fast ion energy determination. Additional dependencies of the confinement time on parameters such as collisionality, plasma beta cannot presently be determined accurately from the data. Although no particular theoretical model can be singled out as a best description of the data, it would appear that some models can be discarded (the scalings of resistive and ideal MHD).

The main result of our study establishes a firm physics foundation for confinement scaling. Any scaling law can and should be cast in a form which embodies the fundamental theoretical constraint imposed by the High-$\beta$ collisional Fokker Planck equation.

## Acknowledgements

This work began after discussions with J. DeBoo, J.W. Connor, M.N. Rosenbluth and P. Lallia. The authors acknowledge the impetus arising from these discussions. Furthermore the study could not have been made possible without data from Tokamaks of *different* sizes. Such data has been made available by the teams of JET, TFTR, JT-60, DIII-D, ASDEX, PDX, JFT2M, PBXM and this is gratefully acknowledged. The authors also thank Drs. R.J. Bickerton and M. Keilhacker for carefully reading this manuscript and for suggesting improvements.

References


[1] YUSHMANOV, P.N., TAKIZUKA, T., RIEDEL, K.S., et al., Nucl. Fusion 30 (1990).

[2] SIGMAR, D.J., BATEMAN, G., BELL, M.G., et al., 13th Conf. on Plasma Physics and Controlled Fusion Research, Washington (1990), IAEA-CN-53-G-1-1.

[3] KAYE, S.M., BARNES, C.W., BELL, M.G., et al, Status of Global Energy Confinement studies, PPPL-2670, Princeton Plasma Physics Laboratory (1990). To be published in Phys. Fluids.

[4] CORDEY, J.G., DEBOO, J., KAYE, S.M., MIURA, Y., et al., Report on ITER H-mode data base, to be submitted to Nucl. Fusion.

[5] REIDEL, K.S., KAYE, S.M., Nucl. Fusion 30 (1990) 731.

[6] BICKERTON, R.J., Univ. of Texas, report FRCR #374, July 1990.

[7] CORDEY, J.G., DEBOO, J., KAYE, S.M., MIURA, Y., et al., Proc. 13th Conf. on Plasma Physics and Controlled Fusion Research, Washington (1990), IAEA-CN-53-F-3-19.

[8] GOLDSTON, R.J., Plasma Physics and Controlled Fusion, 26 (1984) 87.

[9] KAYE, S.M., GOLDSTON, R.J., Nucl. Fusion 25 (1985) 65.

[10] REBUT, P.H., LALLIA, P.P., WATKINS, M.L., in Plasma Physics and Controlled Nuclear Fusion Research 1988 (Proc. 12th Int. Conf. Nice, 1988) Vol. 2, IAEA, Vienna (1989) 191.

[11] ODAJIMA, K., SHIMOMURA, Y., Energy Confinement Scaling based on offset Linear Characteristics, Rep. JAERI-M88-068, Japan Atomic Energy Research Institute, Ibaraki (1988).

[12] CHRISTIANSEN, J.P., CORDEY, J.G., THOMSEN, K., Nucl. Fusion 30 (1990) 1183.

[13] CONNOR, J.W., TAYLOR, J.B., Nucl. Fusion 17 (1977) 1047.

[14] CONNOR, J.W., Plasma Physics and Controlled Fusion 20 (1988) 619.

[15] KADOMTSEV, B.B., Soviet J. Plasma Physics, 1 (1975) 295.

[16] WALTZ, R.E., DEBOO, J.C. ROSENBLUTH, M.N., Phys. Rev. Letter 65 (1990) 2390.

[17] MARDIA, K.V., KENT, J.T., BIBBY, J.M., Multivariate analysis, Academic Press, London (1979).

[18] CHRISTIANSEN, J.P., CORDEY, J.G., MUIR, D.G., Nucl. Fusion 29 (1989) 1505.

[19] WESSON, J.A., Tokamaks, Oxford Science Publications, Clarendon Press, Oxford (1987).

[20] CALLEN, J.D., CHRISTIANSEN, J.P., CORDEY, J.G., THOMAS, P.R., THOMSEN, K., Nucl. Fusion 27 (1987) 1857.

[21] ROMANELLI, F., TANG, W.M., WHITE, R.B., Nucl. Fusion 26 (1986) 1515.

[22] LEE, G.S., DIAMOND, P.H., Phys. Fluids 29 (1986) 3291.

[23] HAGAN, W.K., FRIEMAN, F.A., Phys. Fluids 29 (1986) 3635.

[24] FRIEMAN, E.A., CHEN, LIU, Phys. Fluids 25 (1982) 502.

[25] THOMAS, P.R., A comparison between additional heating data and forms with model scale invariance preprint JET-P(87)17, JET Joint Undertaking, Abingdon, Oxon. (1987).

Appendix 1: Variable sets

This and the three following Appendixes present details of the matrix algebra used to implement the theoretical constraints such that an improved understanding of the content of the Tables should be possible.

All variables used in a regression analysis are standardized to a zero mean value, i.e. for each variable $v_k$ we make the transformation

$$\log v_k \rightarrow \log v_k - \log \bar{v}_k \qquad with \qquad \log \bar{v}_k = \frac{1}{N} \sum_{j=1}^{N} \log v_{kj} \tag{A1.1}$$

In (A1.1) log denotes the natural logarithm and N denotes the number of data values. The variances $s_K$ of the data on the variables $v_K$ are defined as the square root of the k th diagonal element in the empirical data correlation matrix $\underline{S}$, i.e.

$$s_k = \left(S_{kk}\right)^{\frac{1}{2}} \quad \text{where} \quad S_{lk} = \frac{1}{N} \sum_{j=1}^{N} \log v_{lj} \log v_{kj} \tag{A1.2}$$

Table I also lists values of $s_k$ and it can be seen that the H-mode data has in general larger values of $s_k$ than the L-mode data. The use of standardized variables means that the constant C of Eq. (1) drops out as a fitting parameter.

We consider four sets of variables each with one dependent variable $\tau$ referred to by subscript o in formulas and M (= 8) independent variables. The first set referred to as the engineering set, is written as a vector

$$\underline{Z}^t = \log\{\tau, a, n, I, P, \varepsilon, \kappa, A, B\} \tag{A1.3}$$

In the power law representation (Eq. 1) for $\tau$ the associated exponents are denoted by $z_k$, k = 1, M with $z_o$ = - 1. In the paper we use however q, n, etc, as subscripts. The superscript t shows that $\underline{Z}$ itself is a column vector [17].

The set of physics variables is derived from Eqs. (8-10) as

$$\underline{X}^t = \log\{\tau, \tau_B, \rho_*, \nu_*, \beta, \varepsilon, \kappa, A, q\} \tag{A1.4}$$

In the power law representation (Eq. 3) for $\tau$ the associated exponents are denoted by $x_k$, k = 1, M now with $x_o \neq$ - 1, although like above, we use $x_\rho$ etc. in the main sections of the paper. Linear regression cannot be made directly on $\underline{X}$ since the independent

variables contain $\tau$. The omission of $\tau$ from Eqs. (8-10) (denoted by tilde symbol) leads to the regressor variables

$$\underline{Y}^t = \log\{\tau, \tilde{\tau}_B, \tilde{\rho}_*, \tilde{\nu}_*, \beta, \varepsilon, \kappa, A, q\} \qquad (A1.5)$$

The corresponding exponents are denoted by $y_k$ with $y_0 = -1$.

The principal component set is constructed from $\underline{Y}$ by forming certain linear combinations [14]

$$\Phi_k = \sum_{j=1}^{M} \lambda_{jk} Y_j \qquad (A1.6)$$

The covariance matrix $\underline{S}$ of the variables $\Phi k$ is now diagonal. The results of the principal component analysis are summarized by the values $\lambda_{jk}$ given in Tables II and III for L and H-mode data respectively. We notice that the first *two* components are the same for L and H-mode data. These components involve only the parameters with tilde in (A1.5) and they account for 97-98% of the accumulated data variation. Tables II and III also give for each principal component the variance $s_k$, the accumulative proportion of variation $\mu_k$ in units (%), the experimental error $e_k$, the exponent $\bar{\phi}_k$ and its uncertainty $\delta\bar{\phi}_k$ from unconstrained fits, and two "distances" labelled $D_{ITER}$, $D_{CIT}$. All these quantities are defined as follows:

$$s_k = S_{kk}^{\frac{1}{2}} \qquad S_{kk} = \frac{1}{N}\sum_{j=1}^{N} \Phi_k \Phi_k$$

$$\mu_k = S_{kk}\left(\sum_{m=1}^{M} S_{mm}\right)^{-1}$$

$$e_k = \Delta\Phi_k / s_k$$

The experimental error $\Delta\Phi_k$ on a component is computed from the following errors in (A1.3): a (2%), n (10%), I (2%), P (10%), $\varepsilon$ (2%), $\kappa$ (5%), A (0%) and B (2%). The exponents $\bar{\phi}_k$ and $\delta\bar{\phi}_k$ are described in Appendix 2 and so too is the change $\delta\sigma$ to the r.m.s. error caused by omission of a component. The distances $D_{ITER}$ and $D_{CIT}$ are defined as e.g.

$$D_{ITER,k} = \Phi_k(ITER)/s_k$$

since the data base mean $< \Phi_k > \equiv 0$. ITER and CIT parameters [1,2] have been used to evaluate $D_{ITER}$ and $D_{CIT}$.

The normalised distances $D_{ITER}$ and $D_{CIT}$ measure the statistical uncertainties associated with extrapolations from the data base average along each of the eight principal directions. For the L-mode data components 7 and 8, proportional to $a^3/\kappa^4 B^2$ and $a^2/R^3\kappa$ respectively, there is insufficient data variation to warrant extrapolations to both ITER and CIT in the associated directions. For the H-mode data extrapolations to CIT along component 8 proportional to 1/B should not be made.

From Table II we notice that the normalised error $e_8 > 1$ and component 8 should hence be discarded in data analysis.

Appendix 2: Regression

The vectors $\underline{Z}$, $\underline{X}$, $\underline{Y}$, $\underline{\Phi}$ of Appendix 1 are linearly related by

$$\underline{X} = \underline{G}\,\underline{Y} \quad , \quad \underline{X} = \underline{H}\,\underline{Z} \quad , \quad \underline{X} = \left(\underline{\Lambda}\,\underline{G}^t\right)^{-1}\underline{\Phi} \qquad (A2.1)$$

The M + 1 by M + 1 matrices are easily derived from the exponents of a, n etc. in Eqs. (8-10). The matrix $\underline{\Lambda}$ contains the M by M values $\lambda_{jk}$ of (A1.6) plus a column and a row of zeros with a 1 on the diagonal. This matrix is data dependent (see Tables II and III).

Since the variable vectors of (A2.1) are linearly related a regression fit on any of these will yield equivalent results. A power law scaling is formally expressed by any of the following identities

$$< \underline{x}\,\underline{X} > = 0, \quad < \underline{y}\,\underline{Y} > = 0 \quad , \quad < \underline{z}\,\underline{Z} > = 0 \quad , \quad < \underline{\phi}\,\underline{\Phi} > = 0 \qquad (A2.2)$$

The angular brackets refer to data set means and the vector of exponents $\underline{y}$ denotes $\{y_0, y_1, \ldots\ldots y_8\}$ and similarily for $\underline{z}$ and $\underline{\phi}$; the regression eqs. correspond to respectively setting $y_0 \equiv -1$, $z_0 \equiv -1$, $\phi_0 \equiv -1$. It is advantageous (see below) to carry out a regression analysis on the principal components $\underline{\Phi}$ since their covariance matrix is diagonal; this avoids matrix inversion. From the solution $\underline{\phi}$ the other vectors of exponents can then be calculated from

$$\underline{x} = \left(\underline{G}^t\right)^{-1}\underline{\Lambda}^t\,\underline{\phi} \quad , \quad \underline{y} = \underline{\Lambda}^t\,\underline{\phi} \quad , \quad \underline{z} = \underline{H}^t\left(\underline{G}^t\right)^{-1}\underline{\Lambda}^t\,\underline{\phi} \qquad (A2.3)$$

However to obtain the physics representation (Eq. 3) in which $\tau$ appears on both the left and right hand sides we require $x_0 \equiv -1$. The values found from (A2.3) must therefore be normalised via

$$x_k = \frac{y_k}{-x_o} \qquad where \qquad x_o = -1 + y_1 - \tfrac{1}{2} y_2 + 2y_3 - y_4 \qquad (A2.4)$$

A regression analysis minimizes the root mean square error which we denote by $\sigma$ in this paper. Regression on $\underline{\Phi}$ leads to the following simple relations if we augment $\underline{S}^1$ with the elements $S_{ok}$ and $S_{ko}$ given by

$$S_{ok} = \frac{1}{N} \sum_{j=1}^{N} \Phi_o \Phi_k \quad , \quad \Phi_o = \log \tau \quad .$$

The r.m.s. error is then simply expressed as

$$\sigma^2 = S_{oo} + \sum_{k=1}^{M} \left( \phi_k^2 \; S_{kk} - 2\phi_k \; S_{ok} \right)$$

We follow standard rules of statistics and multiply quoted values of $\sigma^2$ by N/(N-M+K) where K is the number of constraints imposed. The unconstrained regression yields for the solution $\bar{\phi}_\kappa$ for its variance $\delta\bar{\phi}_k^2$ and for the minimum r.m.s. error.

$$\bar{\phi}_k = \frac{S_{ok}}{S_{kk}} \quad , \quad \delta\bar{\phi}_k^2 = \frac{\sigma_{\min}^2}{N S_{kk}} \quad , \quad \sigma_{\min}^2 = S_{oo} - \sum_{k=1}^{M} 2\bar{\phi}_k \, S_{kk} \qquad (A2.5)$$

Any constraint imposed will change the solution $\phi_\kappa$ and hence change $\sigma$ to

$\sigma^2 = \sigma_{\min}^2 + \delta\sigma^2$ where

$$\delta\sigma^2 = \sum_{k=1}^{N} S_{kk} \left( \phi_k - \bar{\phi}_k \right)^2 \qquad (A2.6)$$

Table II and III give the values of $\bar{\phi}_k$ and $\delta\,\bar{\phi}_k$ and in addition the change $\delta\sigma = (\delta\sigma^2)^{1/2}$ caused by omission of each principal component in turn; since these are orthogonal omission of one component leaves the remaining values $\bar{\phi}_k$ unchanged.

Appendix 3: Constraints

Let L denote the number of theoretical constraints that are simultaneously imposed on the exponents of a power law expression such as Eq. (1). Appendix 4 presents the actual constraint equations for six theoretical models while this Appendix gives a formula for the change $\delta\sigma^2$ to the r.m.s. error given by (A2.6). The constraint equations (13) for the physics variables $\underline{x}$ can be recast by substituting (A2.3). When $\underline{z}$ is substituted for $\underline{x}$ we get the relations of Appendix 4. If we substitute for $\underline{\phi}$ we get

$$\underline{C}\,\underline{x} = \underline{C}\,\left(\underline{G}^t\right)^{-1}\,\underline{\Lambda}^t\,\underline{\phi} = \underline{D}\,\underline{\phi} = 0 \qquad (A3.1)$$

or

$$\sum_{k=o}^{M} D_{\ell k}\,\phi_k = 0 \quad , \quad \ell = 1,2 \ldots \mathrm{K} \qquad (A3.2)$$

in which $\phi_o = -1$.

The coefficients $D_{\ell k}$ are data dependent and need to be computed. The change to the unconstrained solution $\bar{\phi}_k$ (A2.5) becomes

$$\delta\phi_k = \phi_k - \bar{\phi}_k = \sum_{\ell=1}^{\mathrm{K}} \lambda_\ell\,\frac{D_{\ell k}}{2S_{kk}} \qquad (A3.3)$$

The Langrange multipliers $\lambda_\ell$ satisfy the linear equations for $\ell = 1, \ldots \mathrm{K}$

$$U_\ell + \sum_{i=1}^{\mathrm{K}} W_{\ell i}\,\lambda_i = D_{\ell o} \qquad (A3.4)$$

where

$$U_\ell = \sum_{k=1}^{M} D_{\ell k}\,\bar{\phi}_k \qquad \textit{and} \qquad W_{ij} = \sum_{k=1}^{M} D_{ik}\,D_{jk}\left(2\,S_{kk}\right)^{-1}$$

The change $\delta\sigma^2$ to the r.m.s. error arising from the constraint equations (A3.2) is obtained by inserting (A3.3 into (A2.6)

$$\delta\sigma^2 = \sum_{k=1}^{M} \tfrac{1}{4}\,S_{kk}^{-1}\left(\sum_{\ell=1}^{\mathrm{K}} \lambda_\ell\,D_{\ell k}\right)^2 \qquad (A3.5)$$

The F-test [17] examines if $\delta\sigma^2 < \sigma^2_{min}/N$ per constraint. This can be satisfied if for a principal component n involved in the test, $S_{nn} << S_{kk}$, k = 1, M, k ≠ n. In that case the weight coefficients $W_{ij}$ and hence the Lagrange multipliers $\lambda_\ell$ are largely determined by the component n. Thus to satisfy a constraint with $|\delta\phi_n| >> |\delta\phi_k|$, k ≠ n, requires $\delta\sigma^2 \approx S_{nn}\,\delta\phi^2_n < \sigma^2_{min}\frac{1}{N}$. To illustrate this point we consult Tables II and IV. We notice that the long wavelength scaling constraint is satisfied by the L-mode data. This is achieved via $\delta\phi_8 = -0.43$ while $|\delta\phi_K| < 0.005$ for k ≠ 8. Table II shows however that component 8 can be omitted; without the principal component 8 the constraint can no longer be satisfied. Thus artefacts in data can lead to false conclusions on statistical grounds.

Appendix 4: Transport models

In this Appendix we list the constraint equations for six theoretical transport models in terms of the x, y, z exponents. To make the interpretation easier we use subscripts a, n, I etc for z. (Notice that $y_0 = -1$ in the equations and that f denotes some function as expressed by Eq. (2)).

The High β collisional model:

$\tau_{theory} = \tau_B f$. This constraint expressed by Eq. (20) and first derived by Kadomtsev [15] applies to all the theoretical models considered. The resulting scaling of τ becomes dimensionally correct [13] and can also be expressed as $\Omega_c^{-1}\,\rho_*^{-2}$ where $\Omega_c$ is the cyclotron frequency. The constraint implies the following relations between the x, y, z exponents

$$x_0 + x_1 = 0 \quad , \quad y_0 + 2y_1 - 1/2y_2 + 2y_3 - y_4 = 0$$

$$4z_a - 8z_n - 8z_n - z_I - 3z_p - 5z_B = 5$$

Gyro-Bohm scaling:

$\tau_{theory} = \tau_B\,\rho_*^{-1} f$. This scaling has been derived by Hagan and Freeman [23] and by Connor [14]. The transport arises from turbulent fluctuations with frequencies $\omega << \Omega_{ci}$ and it is described by the ion gyro-kinetic equation of Freeman and Chen [24]. The scale lengths of the fluctuations are of order $\rho_i$ and the confinement scaling has been referred to as the short wavelength gyrokinetic transport scaling. The additional constraint is

$$x_1 + x_2 = 0 \quad , \quad y_1 + y_2 = 0$$

$$6z_a - 22z_n - 9z_1 - 12z_\rho - 15z_B = 0$$

Bohm scaling:

$\tau_{theory} = \tau_B \rho_*^0$ f. This scaling is similar to the one above but the fluctuation scale lengths are of order a, hence it can be referred to as the long wavelength gyrokinetic transport scaling with the additional constraint.

$$x_2 = 0 \quad , \quad y_2 = 0$$

$$2z_a - 14z_n - 8z_I - 14z_\rho - 10z_B = 0$$

Resistive MHD:

$\tau_{theory} = \tau_B \rho_*^1 \beta^{1/2}$ f. This scaling derived from MHD equations by Connor [14] and Thomas [25] replaces $\nu_*$ in the f function by $\nu_* \rho_*^2$. Unlike the gyrokinetic models the MHD scalings imply a positive exponent for the $\rho_*$ term. This corresponds to

$$x_0 + x_2 - 2x_3 = 0 \quad , \quad y_0 + y_1 + 1/2y_2 - y_4 = 0$$

$$4z_a - 18z_n - 6z_I - 13z_\rho - 10z_B = 0$$

Ideal MHD:

$\tau_{theory} = \tau_B \rho_*^1 \beta^{1/2} \nu_*^0$ f. The ideal MHD scaling is similar to the resistive MHD one but it imposes one extra constraint since collisional effects are eliminated. This scaling has been studied by Bickerton [6]. The first constraint is

$$x_1 - x_2 = 0 \quad , \quad y_1 - y_2 = 0$$

$$2z_a - 6z_n + 7z_I + 16z_\rho + 5z_B = 0$$

The absent scaling with $\nu_*$ is expressed as

$$x_3 = 0 \quad , \quad y_3 = 0$$

$$-z_a + 2z_n - z_I - 3z_\rho = 0$$

Resistive fluid turbulence:

$\tau_{theory} = \tau_B \rho_*^{-1} \beta^{1/2} \nu_*^{-1} f$. This model derived from fluid equations has basically the same form as that of gyro-Bohm scaling but with a specific $\nu_*$ dependence. Thus

$$x_1 + x_2 = 0 \quad , \quad y_1 + y_2 = 0$$

$$6z_a - 22z_n - z_1 - 3z_I - 15z_B = 0$$

and the fixed scaling with $\nu_*$ corresponds to

$$x_0 - x_3 = 0 \quad , \quad y_0 + y_1 - 1/2y_2 + y_3 - y_4 = 0$$

$$z_a + 2z_n - z_I - 3z_p = 0$$

| Variable | | L-mode | $s_k$ | H-mode | $s_k$ |
|---|---|---|---|---|---|
| Minor radius (m) | a | 0.24 - 1.21 | 0.34 | 0.24 - 1.21 | 0.62 |
| Density ($10^{19}$ m$^{-3}$) | n | 0.83 - 11.9 | 0.48 | 0.56 -12.5 | 0.28 |
| Plasma current (MA) | I | 0.11 - 5.10 | 0.62 | 0.12 - 5.16 | 1.15 |
| Total power (MW) | P | 0.33 - 23.1 | 0.84 | 0.37 - 18.3 | 0.88 |
| Elongation | $\kappa$ | 1 - 1.9 | 0.18 | 1 - 2.0 | 0.30 |
| Aspect ratio | $\varepsilon$ | 0.21 - 0.37 | 0.18 | 0.17 - 0.37 | 0.22 |
| Ion mass number | A | 1 - 2 | 0.33 | 1 - 2 | 0.18 |
| Beam mass number | $A_b$ | 1 -2 | | 1 - 2 | |
| Safety factor | q | 1.46 - 9.10 | 0.25 | 0.51 - 5.83 | 0.23 |
| Toroidal field (T) | B | 0.64 - 5.15 | 0.37 | 0.77 - 3.71 | 0.29 |
| Plasma energy (MJ) | W | 0.004 - 5.23 | 1.22 | 0.013 - 10.2 | 2.21 |
| Confinement time (s) | $\tau$ | 0.005 - 0.95 | 0.86 | 0.015 - 1.43 | 1.36 |
| Bohm time (ms) | $\tau_B$ | 0.027 - 0.60 | 0.60 | 0.009 - 0.56 | 1.25 |
| Larmor radius | $\rho_*$ | 0.005 - 0.27 | 0.44 | 0.005 - 0.09 | 0.87 |
| Collisionality | $\nu_*$ | 0.0014 - 0.3 | 0.91 | 0.0017 - 0.7 | 1.01 |
| Beta poloidal | $\beta$ | 0.08 - 2.3 | 0.35 | 0.09 - 2.3 | 0.53 |

**Table I.** *Ranges of basic parameters in the ITER L and H-mode data bases. The variances $s_k$ (see Appendix 1) are larger for most of the H-mode data than for the L-mode data.*

| L | $\tilde{\tau}_B$ | $\tilde{\rho}_*$ | $\tilde{\nu}_*$ | $\tilde{\beta}_*$ | $\varepsilon$ | $\kappa$ | A | q |
|---|---|---|---|---|---|---|---|---|
| 1 | 0.61 | -0.35 | 0.51 | -0.49 | 0.07 | 0.04 | 0.08 | 0.03 |
| 2 | -0.25 | 0.19 | 0.85 | 0.42 | 0.06 | 0.02 | -0.05 | -0.07 |
| 3 | -0.26 | 0.38 | 0.07 | -0.38 | 0.15 | 0.34 | 0.68 | 0.25 |
| 4 | 0.33 | -0.02 | -0.04 | 0.46 | 0.11 | –0.06 | 0.09 | 0.80 |
| 5 | 0.14 | -0.29 | -0.07 | 0.39 | 0.02 | –0.27 | 0.71 | -0.40 |
| 6 | 0.30 | 0.02 | -0.10 | 0.31 | 0.26 | 0.80 | -0.09 | -0.28 |
| 7 | 0.49 | 0.77 | -0.03 | -0.01 | 0.11 | –0.32 | -0.03 | -0.22 |
| 8 | -0.20 | -0.12 | 0.04 | -0.03 | 0.94 | 0.22 | -0.12 | -0.03 |

| L | s | $\mu$ | e | $\bar{\phi}$ | $\delta\bar{\phi}$ | $\delta\sigma$ (%) | $D_{ITER}$ | $D_{CIT}$ |
|---|---|---|---|---|---|---|---|---|
| 1 | 5.64 | 91.5 | 0.15 | 0.372 | 0.001 | 79.09 | 2.92 | 1.39 |
| 2 | 0.30 | 4.95 | 0.48 | -0.169 | 0.007 | 3.80 | 2.08 | 1.14 |
| 3 | 0.11 | 1.82 | 0.09 | 0.267 | 0.011 | 4.54 | 2.06 | 0.43 |
| 4 | 0.06 | 1.04 | 0.30 | 0.070 | 0.015 | 0.16 | 0.84 | 3.89 |
| 5 | 0.02 | 0.35 | 0.25 | -0.355 | 0.025 | 1.35 | 4.81 | 1.51 |
| 6 | 0.015 | 0.24 | 0.32 | -0.063 | 0.030 | 0.03* | 5.17 | 0.58 |
| 7 | 0.001 | 0.02 | 0.70 | 0.122 | 0.096 | 0.004* | 8.59 | 16.75 |
| 8 | $4\ 10^{-4}$ | 0.007 | 1.15 | -0.086 | 0.172 | 0.0* | 19.3 | 12.5 |

**Table II.** *The values of $\lambda_{jk}$ (see Eq. (A1.6)) for the principal components in L-mode data are given in the top half of this Table. The lower half gives values for each component of parameters defined in Appendixes 1, 2 and 3. The asterisks indicate that omission of either component 6 or 7 or 8 satisfies the F-test.*

| H | $\tilde{\tau}_B$ | $\tilde{\rho}_*$ | $\tilde{\nu}_*$ | $\tilde{\beta}$ | $\varepsilon$ | $\kappa$ | A | q |
|---|---|---|---|---|---|---|---|---|
| 1 | 0.62 | -0.37 | 0.52 | -0.44 | 0.07 | 0.02 | 0.02 | 0.03 |
| 2 | -0.25 | 0.26 | 0.82 | 0.40 | -0.01 | -0.03 | -0.17 | -0.01 |
| 3 | 0.36 | 0.08 | -0.14 | 0.35 | 0.36 | -0.21 | -0.35 | 0.65 |
| 4 | 0.21 | -0.28 | 0.0 | 0.58 | -0.15 | 0.25 | 0.66 | 0.13 |
| 5 | -0.16 | 0.38 | 0.10 | -0.39 | -0.05 | -0.27 | 0.55 | 0.52 |
| 6 | -0.03 | 0.09 | 0.0 | -0.14 | -0.48 | 0.68 | -02.8 | 0.42 |
| 7 | -0.28 | -0.05 | 0.05 | -0.12 | 0.77 | 0.53 | 0.14 | 0.06 |
| 8 | 0.51 | 0.74 | -0.06 | 0.04 | 0.09 | 0.23 | 0.10 | -0.33 |

| H | s | $\mu$ | e | $\bar{\phi}$ | $\delta\bar{\phi}$ | $\delta\sigma$ (%) | $D_{ITER}$ | $D_{CIT}$ |
|---|---|---|---|---|---|---|---|---|
| 1 | 20.1 | 97.8 | 0.08 | 0.335 | 0.001 | 139.1 | 2.29 | 1.46 |
| 2 | 0.31 | 1.5 | 0.45 | -0.336 | 0.008 | 10.16 | 0.05 | 2.86 |
| 3 | 0.07 | 0.3 | 0.17 | -0.404 | 0.017 | 4.17 | 1.12 | 2.53 |
| 4 | 0.03 | 0.1 | 0.36 | 0.440 | 0.027 | 2.16 | 2.95 | 2.28 |
| 5 | 0.017 | 0.08 | 0.20 | 0.571 | 0.035 | 2.13 | 4.28 | 0.21 |
| 6 | 0.010 | 0.05 | 0.50 | 0.805 | 0.046 | 2.48 | 1.55 | 0.24 |
| 7 | 0.003 | 0.02 | 0.51 | -1.550 | 0.082 | 2.87 | 5.44 | 0.35 |
| 8 | 0.001 | 0.01 | 0.19 | 0.114 | 0.114 | 0.39 | 1.67 | 7.93 |

**Table III.** *The values of $\lambda_{jk}$ (see Eq. (A1.6)) for the principal components in H-mode data are given in the top half of this Table. The lower half gives values for each component of parameters defined in Appendixes 1, 2 and 3.*

| Data selected | $\tau_{total}$ (L) | $\tau$ (L) | $\tau_{total}$ ($L_8$) | $\tau_{total}$ (H) | $\tau$ (H) |
|---|---|---|---|---|---|
| No. of data values | 680 | 680 | 680 | 693 | 693 |
| Unconstrained $\sigma_{min}$ | 8.85 | 9.60 | 9.60 | 11.65 | 12.42 |

| Data selected | $\delta\sigma$ | $\delta\sigma$ | $\delta\sigma$ | $\delta\sigma$ | $\delta\sigma$ |
|---|---|---|---|---|---|
| High $\beta$ collisional | 0.02* | 0.0* | 0.0* | 0.0* | 0.01* |
| Short wavelength | 1.98 | 0.65 | 2.36 | 0.28 | 0.24 |
| Long wavelength | 0.84 | 0.09* | 0.65 | 0.40 | 1.57 |
| Resistive MHD | 0.02* | 0.78 | 1.46 | 1.00 | 2.83 |
| Ideal MHD | 0.04* | 1.83 | 1.91 | 3.49 | 3.03 |
| Res. fl. turbulence | 9.83 | 8.37 | 9.52 | 7.11 | 5.67 |

**Table IV.** *The changes in the root mean square errors $\delta\sigma$ (in units %) caused by imposing the constraints of six theoretical models. The top part gives the minimum rmse obtained with an unconstrained fit to $\tau_{total}$ or $\tau$ as shown. $L_8$ means that principal component 8 is omitted. The asterisks indicate those constraints satisfied by the tests (15-16). The values for the exponents $x_\tau$ etc. of Eq. (3) which result from imposing these constraints are given in Table V.*

| L-mode | $x_\tau$ | $x_\rho$ | $x_\nu$ | $x_\beta$ | $x_\varepsilon$ | $x_\kappa$ | $x_A$ | $x_q$ |
|---|---|---|---|---|---|---|---|---|
| Unconstrained | 1.13 | 0.71 | 0.42 | -2.30 | -0.03 | 0.60 | -0.07 | 1.39 |
| High-$\beta$ coll. | 1 | 0.56 | 0.42 | -2.28 | 0.14 | 0.59 | -0.08 | 1.40 |
| Long | 1 | 0 | 0.35 | -2.12 | -2.11 | 1.42 | 0.25 | 1.66 |

| H-mode | $x_\tau$ | $x_\rho$ | $x_\nu$ | $x_\beta$ | $x_\varepsilon$ | $x_\kappa$ | $x_A$ | $x_q$ |
|---|---|---|---|---|---|---|---|---|
| Unconstrained | 0.68 | -2.21 | -0.08 | -1.38 | -7.46 | -1.58 | 1.13 | 2.39 |
| High-$\beta$ coll. | 1 | -1.77 | -0.12 | -1.33 | -7.49 | -1.53 | 1.16 | 2.19 |
| Short | 1 | -1 | -0.15 | -1.30 | -5.58 | -0.53 | 1.29 | 1.77 |

**Table V.** *Values of the exponents $x_\tau$ etc. of Eq. (3) obtained when imposed theoretical constraints are satisfied by the data. Notice the difference in the $\nu^*$ dependence between L and H-mode data.*

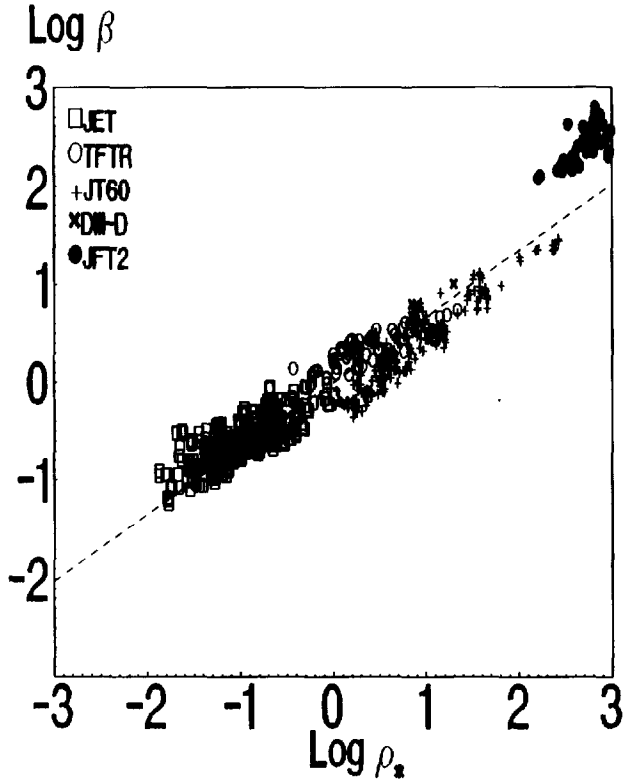


*FIG. 1. Collinearity in the ITER L-mode data. The tilde refers to the omission of τ from β ρ* in Eqs.(8-9). Log denotes the natural logarithm (data-base mean is zero).*

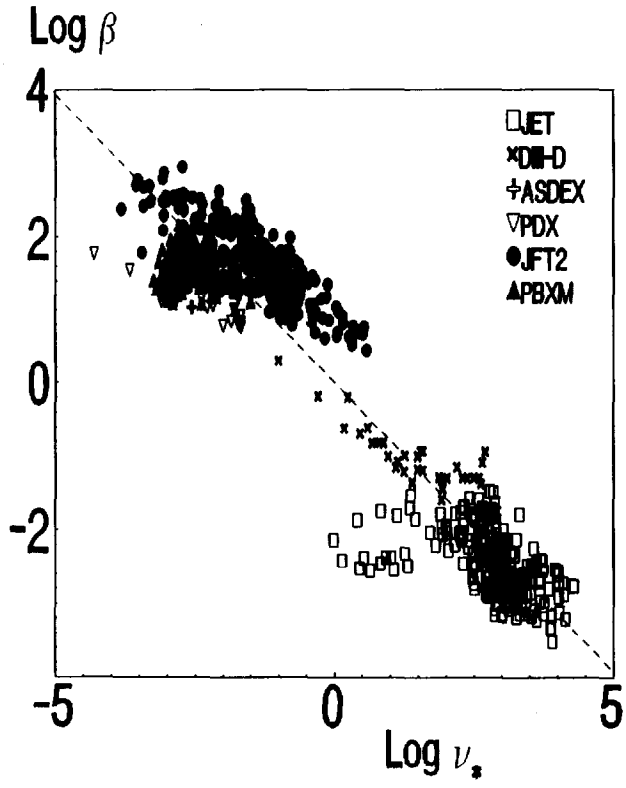


*FIG. 2. Collinearity in the ITER H-mode data. The tilde refers to the omission of τ from β ν* in Eqs.(8-9). Log denotes the natural logarithm (data-base mean is zero).*

# APPENDIX 1.

## THE JET TEAM

JET Joint Undertaking, Abingdon, Oxon, OX14 3EA, U.K.

J.M.Adams[1], F.Alladio[4], H.Altmann, R.J.Anderson, G.Appruzzese, W.Bailey, B.Balet, D.V.Bartlett, L.R.Baylor[24], K.Behringer, A.C.Bell, P.Bertoldi, E.Bertolini, V.Bhatnagar, R.J.Bickerton, A.Boileau[3], T.Bonicelli, S.J.Booth, G.Bosia, M.Botman, D.Boyd[31], H.Brelen, H.Brinkschulte, M.Brusati, T.Budd, M.Bures, T.Businaro[4], H.Buttgereit, D.Cacaut, C.Caldwell-Nichols, D.J.Campbell, P.Card, J.Carwardine, G.Celentano, P.Chabert[27], C.D.Challis, A.Cheetham, J.Christiansen, C.Christodoulopoulos, P.Chuilon, R.Claesen, S.Clement[30], J.P.Coad, P.Colestock[6], S.Conroy[13], M.Cooke, S.Cooper, J.G.Cordey, W.Core, S.Corti, A.E.Costley, G.Cottrell, M.Cox[7], P.Cripwell[13], F.Crisanti[4], D.Cross, H.de Blank[16], J.de Haas[16], L.de Kock, E.Deksnis, G.B.Denne, G.Deschamps, G.Devillars, K.J.Dietz, J.Dobbing, S.E.Dorling, P.G.Doyle, D.F.Düchs, H.Duquenoy, A.Edwards, J.Ehrenberg[14], T.Elevant[12], W.Engelhardt, S.K.Erents[7], L.G.Eriksonn[5], M.Evrard[2], H.Falter, D.Flory, M.Forrest[7], C.Froger, K.Fullard, M.Gadeberg[11], A.Galetsas, R.Galvao[8], A.Gibson, R.D.Gill, A.Gondhalekar, C.Gordon, G.Gorini, C.Gormezano, N.A.Gottardi, C.Gowers, B.J.Green, F.S.Griph, M.Gryzinski[26], R.Haange, G.Hammett[6], W.Han[9], C.J.Hancock, P.J.Harbour, N.C.Hawkes[7], P.Haynes[7], T.Hellsten, J.L.Hemmerich, R.Hemsworth, R.F.Herzog, K.Hirsch[14], J.Hoekzema, W.A.Houlberg[24], J.How, M.Huart, A.Hubbard, T.P.Hughes[32], M.Hugon, M.Huguet, J.Jacquinot, O.N.Jarvis, T.C.Jernigan[24], E.Joffrin, E.M.Jones, L.P.D.F.Jones, T.T.C.Jones, J.Källne, A.Kaye, B.E.Keen, M.Keilhacker, G.J.Kelly, A.Khare[15], S.Knowlton, A.Konstantellos, M.Kovanen[21], P.Kupschus, P.Lallia, J.R.Last, L.Lauro-Taroni, M.Laux[33], K.Lawson[7], E.Lazzaro, M.Lennholm, X.Litaudon, P.Lomas, M.Lorentz-Gottardi[2], C.Lowry, G.Magyar, D.Maisonnier, M.Malacarne, V.Marchese, P.Massmann, L.McCarthy[28], G.McCracken[7], P.Mendonca, P.Meriguet, P.Micozzi[4], S.F.Mills, P.Millward, S.L.Milora[24], A.Moissonnier, P.L.Mondino, D.Moreau[17], P.Morgan, H.Morsi[14], G.Murphy, M.F.Nave, M.Newman, L.Nickesson, P.Nielsen, P.Noll, W.Obert, D.O'Brien, J.O'Rourke, M.G.Pacco-Düchs, M.Pain, S.Papastergiou, D.Pasini[20], M.Paume[27], N.Peacock[7], D.Pearson[13], F.Pegoraro, M.Pick, S.Pitcher[7], J.Plancoulaine, J-P.Poffé, F.Porcelli, R.Prentice, T.Raimondi, J.Ramette[17], J.M.Rax[27], C.Raymond, P-H.Rebut, J.Removille, F.Rimini, D.Robinson[7], A.Rolfe, R.T.Ross, L.Rossi, G.Rupprecht[14], R.Rushton, P.Rutter, H.C.Sack, G.Sadler, N.Salmon[13], H.Salzmann[14], A.Santagiustina, D.Schissel[25], P.H.Schild, M.Schmid, G.Schmidt[6], R.L.Shaw, A.Sibley, R.Simonini, J.Sips[16], P.Smeulders, J.Snipes, S.Sommers, L.Sonnerup, K.Sonnenberg, M.Stamp, P.Stangeby[19], D.Start, C.A.Steed, D.Stork, P.E.Stott, T.E.Stringer, D.Stubberfield, T.Sugie[18], D.Summers, H.Summers[20], J.Taboda-Duarte[22], J.Tagle[30], H.Tamnen, A.Tanga, A.Taroni, C.Tebaldi[23], A.Tesini, P.R.Thomas, E.Thompson, K.Thomsen[11], P.Trevalion, M.Tschudin, B.Tubbing, K.Uchino[29], E.Usselmann, H.van der Beken, M.von Hellermann, T.Wade, C.Walker, B.A.Wallander, M.Walravens, K.Walter, D.Ward, M.L.Watkins, J.Wesson, D.H.Wheeler, J.Wilks, U.Willen[12], D.Wilson, T.Winkel, C.Woodward, M.Wykes, I.D.Young, L.Zannelli, M.Zarnstorff[6], D.Zasche[14], J.W.Zwart.

### PERMANENT ADDRESS

1. UKAEA, Harwell, Oxon. UK.
2. EUR-EB Association, LPP-ERM/KMS, B-1040 Brussels, Belgium.
3. Institute National des Récherches Scientifique, Quebec, Canada.
4. ENEA-CENTRO Di Frascati, I-00044 Frascati, Roma, Italy.
5. Chalmers University of Technology, Göteborg, Sweden.
6. Princeton Plasma Physics Laboratory, New Jersey, USA.
7. UKAEA Culham Laboratory, Abingdon, Oxon. UK.
8. Plasma Physics Laboratory, Space Research Institute, Sao José dos Campos, Brazil.
9. Institute of Mathematics, University of Oxford, UK.
10. CRPP/EPFL, 21 Avenue des Bains, CH-1007 Lausanne, Switzerland.
11. Risø National Laboratory, DK-4000 Roskilde, Denmark.
12. Swedish Energy Research Commission, S-10072 Stockholm, Sweden.
13. Imperial College of Science and Technology, University of London, UK.
14. Max Planck Institut für Plasmaphysik, D-8046 Garching bei München, FRG.
15. Institute for Plasma Research, Gandhinagar Bhat Gujat, India.
16. FOM Instituut voor Plasmafysica, 3430 Be Nieuwegein, The Netherlands.
17. Commissiariat à L'Energie Atomique, F-92260 Fontenay-aux-Roses, France.
18. JAERI, Tokai Research Establishment, Tokai-Mura, Naka-Gun, Japan.
19. Institute for Aerospace Studies, University of Toronto, Downsview, Ontario, Canada.
20. University of Strathclyde, Glasgow, G4 ONG, U.K.
21. Nuclear Engineering Laboratory, Lapeenranta University, Finland.
22. JNICT, Lisboa, Portugal.
23. Department of Mathematics, Univeristy of Bologna, Italy.
24. Oak Ridge National Laboratory, Oak Ridge, Tenn., USA.
25. G.A. Technologies, San Diego, California, USA.
26. Institute for Nuclear Studies, Swierk, Poland.
27. Commissiariat à l'Energie Atomique, Cadarache, France.
28. School of Physical Sciences, Flinders University of South Australia, South Australia SO42.
29. Kyushi University, Kasagu Fukuoka, Japan.
30. Centro de Investigaciones Energeticas Medioambientales y Techalogicas, Spain.
31. University of Maryland, College Park, Maryland, USA.
32. University of Essex, Colchester, UK.
33. Akademie de Wissenschaften, Berlin, DDR.

CR 88.49.1A